

OPEN

Radiation reaction as an energy enhancement mechanism for laser-irradiated electrons in a strong plasma magnetic field

Z. Gong^{1,2}, F. Mackenroth^{3,4}, X. Q. Yan¹ & A. V. Arefiev^{4,5*}

Conventionally, friction is understood as a mechanism depleting a physical system of energy and as an unavoidable feature of any realistic device involving moving parts. In this work, we demonstrate that this intuitive picture loses validity in nonlinear quantum electrodynamics, exemplified in a scenario where spatially random friction counter-intuitively results in a highly directional energy flow. This peculiar behavior is caused by radiation friction, i.e., the energy loss of an accelerated charge due to the emission of radiation. We demonstrate analytically and numerically how radiation friction can dramatically enhance the energy gain by electrons from a laser pulse in a strong magnetic field that naturally arises in dense laser-irradiated plasma. We find the directional energy boost to be due to the transverse electron momentum being reduced through friction whence the driving laser can accelerate the electron more efficiently. In the considered example, the energy of the laser-accelerated electrons is enhanced by orders of magnitude, which then leads to highly directional emission of gamma-rays induced by the plasma magnetic field.

For an accelerated particle of charge q and mass m the main energy dissipation, or friction, is the continuous emission of electromagnetic radiation, referred to as *radiation friction* (RF). The energy loss per unit time is given by¹

$$P = \frac{2q^2 \varepsilon^2}{3m^4 c^7} \left(\frac{dp^\mu}{dt} \right)^2, \quad (1)$$

where c is the speed of light, p^μ is the particle relativistic momentum, ε is its energy, and t is time. Several structural peculiarities of RF were described, e.g., mathematically ill-behaved particle dynamics² or the need for charge renormalization in classical electrodynamics³. For RF to reduce a particle's energy ε at a rate corresponding to the particles' momentum change due to acceleration, the emitted power $P = d\varepsilon/dt = (d\varepsilon/d|\mathbf{p}|)(d|\mathbf{p}|/dt)$, with the particle momentum \mathbf{p} , needs to match the accelerating force, resulting in $|\mathbf{F}_{RF}| = |dp/dt| \sim 3m^4 c^8 / 2\varepsilon^2 q^2$. Early studies deemed this regime of *instantaneous RF* unreachable in a lab, as it would require accelerating electromagnetic fields $E_{RF} \geq F_{RF}/|e| \sim 10^{15}$ V/m even for an electron (the lightest particle) at mildly relativistic energies of $\varepsilon_e \sim 100 m_e c^2$. Such field strengths, however, are becoming increasingly available due to the advent of ultra-high intensity lasers^{4,5} providing intensities $I_L \gtrsim 10^{22}$ W/cm² at optical wavelengths ($\lambda_L \sim 1 \mu\text{m}$), corresponding to electric fields $E_L \gtrsim 10^{15}$ V/m⁶, with facilities aiming at higher fields under construction^{7,8}, sparking renewed interest in instantaneous RF^{9–11}. At these facilities, even experimental observation of the instantaneous RF became possible^{12,13} in the random energy loss of a laser-accelerated relativistic electron bunch when scattered by a high-power laser pulse. Similar setups were investigated in a series of theoretical studies^{14–26}, indicating the acceleration of electrons as an important field of application for high-intensity laser facilities^{27–30}.

The radiation friction has been actively studied due to its non-trivial and sometimes unexpected impact on electron dynamics in strong laser fields^{31–36}. One unexpected effect revealed through an exact solution of the

¹SKLNPT, KLHEDP and CAPT, School of Physics, Peking University, Beijing, 100871, China. ²Center for High Energy Density Science, The University of Texas at Austin, Austin, TX, 78712, USA. ³Max Planck Institute for the Physics of Complex Systems, 01187, Dresden, Germany. ⁴Department of Mechanical and Aerospace Engineering, University of California at San Diego, La Jolla, CA, 92093, USA. ⁵Center for Energy Research, University of California at San Diego, La Jolla, CA, 92093, USA. *email: aarefiev@eng.ucsd.edu

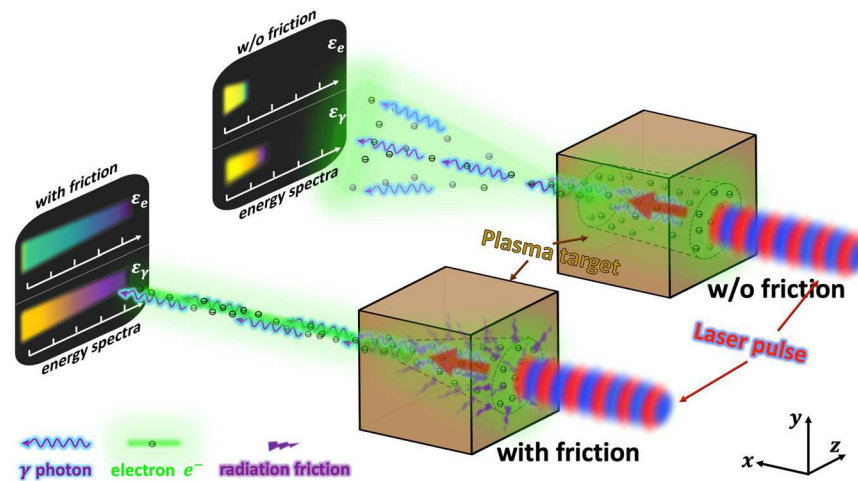


Figure 1. Schematic diagram summarizing the effect of the radiation friction in laser-irradiated plasmas. The green dots are the laser-irradiated electrons, the blue wavy lines are the emitted photons, and the purple fragments are the radiation friction force. Red arrows indicate the direction of the electron beam's acceleration and the black dashed lines mark the location of the magnetic boundary associated with the plasma magnetic field that limits transverse electrons oscillations. Spectra of electron and photon energies, ε_e and ε_γ , (black panels to the left) and their beam divergence (cones left of plasma targets) visualize the pronounced enhancement in peak energies and beam collimation due to the radiation friction.

Landau-Lifshitz equation³⁷ is the energy increase of an electron irradiated by a plane electromagnetic wave^{38–40}. Even though this is a profound result, its impact on laboratory studies of high-intensity laser plasma interactions is limited by the requirement of a large distance and a large transverse spread needed to accelerate electrons to high energies.

In this work, we examine the dynamics of laser-irradiated electrons in the presence of a strong quasi-static magnetic field that naturally arises in a dense plasma irradiated by an ultra-high intensity laser^{41–43}. We demonstrate analytically and numerically how the radiation friction dramatically enhances the electron energy gain in this setup by reducing initial transverse electron momentum and enabling a subsequent efficient energy transfer from the laser field to the electron, as schematically shown in Fig. 1. In contrast to the already discussed energy enhancement in a vacuum, the electrons are accelerated without an increase of their transverse displacement, making it easier to realize the described regime experimentally. A direct benefit of the transverse electron confinement is that the accelerated electrons are directed forward with a small angular spread, which then leads to highly directional gamma-ray emission induced by the plasma magnetic field.

Main Model

This work is motivated by a regime of light-matter interaction where an ultra-high intensity laser pulse is able to propagate through a dense plasma and drive a quasi-static magnetic filament⁴¹. The laser pulse hitting a solid target quickly ionizes the material, turning it into a plasma with an electron density n_e . We consider densities close to the critical threshold $n_c = \pi m_e c^2 / (\lambda_L^2 e^2)$, above which a low-intensity laser pulse with a vacuum wavelength λ_L cannot propagate into the plasma. In an ultra-intense laser pulse, electrons oscillate relativistically, yielding an effective mass increase that extends the cutoff density to $n_c \bar{\varepsilon}_e / m_e c^2 \approx a_0 n_c$. Here a_0 is the normalized laser amplitude defined in terms of the laser intensity and wavelength as $a_0 \equiv \sqrt{I_L [\text{W}/\text{cm}^2]} / 1.37 \times 10^{18} \lambda_L [\mu\text{m}]$. The described effect is referred to as the relativistically induced transparency^{44–48}. It makes it possible for an intense laser pulse to propagate through a dense plasma. The relativistic transparency is important at $I_L \gg 10^{18} \text{ W}/\text{cm}^2$ for $\lambda_L \sim 1 \mu\text{m}$ or, equivalently, at $a_0 \gg 1$.

Particle-in-cell simulations performed by multiple groups have shown that this regime enables generation of strong quasi-static magnetic fields^{49–53}. As the laser pulse propagates through the plasma, it pushes the electrons forward and drives a longitudinal current. The current density scales as $n_e v$, so it can be greatly enhanced by leveraging the relativistic transparency to propagate the laser in a plasma with $n_e \geq n_c$. The longitudinal current is typically distributed over the cross-section of the laser beam, whereas the return current is concentrated at the periphery of the beam. The feature that is of central importance to the present manuscript is the magnetic field that is generated and sustained by the laser-driven current. The field is azimuthal and it forms a magnetic filament co-located with the laser beam.

Additional studies have shown that the laser propagation becomes unstable in a dense relativistically transparent target⁵⁴, which makes the direction of the laser beam propagation unpredictable. One way to suppress the instability while retaining the advantages of laser propagation through a dense plasma is to use structured targets that provide optical guiding to the laser pulse. Here we consider the design where the target consists of a cylindrical channel that is filled with a material that becomes more transparent than the bulk when irradiated by a high intensity laser beam. The channel serves as an optical wave-guide to the beam that is focused at the channel entrance. Structured targets with an initially empty channel have already been used experimentally to achieve

greater control over laser interactions with solid-density targets⁵⁵. Advanced target manufacturing facilities are also able to produce solid targets of variable density using the *in situ* polymerization technique⁵⁶. The pore and thread structures are sub-micron, so a relatively homogeneous plasma with $n_e \geq 0.9n_c$ has been achieved in experiments with high-intensity lasers⁵⁷. It is challenging but feasible to manufacture targets with pre-filled channels, so our study is performed in anticipation of this capability becoming available for experiments at high intensity laser facilities.

The effect of the radiation friction considered here is directly linked to the electron dynamics in the combined laser and plasma fields present in the channel of a structured target^{41,43}. We make use of a simplified model capturing all essential physics, as demonstrated in detailed kinetic plasma simulations^{41–43}. These simulations motivate the following fundamental assumptions underlying the model: (i) Since transverse electron oscillations are confined narrower than the width of the laser beam and the laser's phase fronts inside the channel are near-flat, the electron effectively experiences it as a plane wave. (ii) Since laser beam diffraction is suppressed in structured targets^{41,43}, the laser maintains its peak amplitude over distances much longer than its Rayleigh range. (iii) Dephasing between the electrons and the laser is primarily determined by the longitudinal electron velocity v_x whence we neglect deviations of the phase velocity v_{ph} from c that arise from the laser propagation through a finite-width channel filled with a plasma. It has been shown that the relativistically induced transparency significantly reduces the effect of the plasma on v_{ph} ³⁰. (iv) The laser drives a strong, uniform longitudinal electron current density $j_0 < 0$, with the return current flowing on the periphery of the channel. (v) The quasi-static radial electric field in the channel is much weaker than the azimuthal magnetic field due to the transverse ion mobility that reduces the charge separation caused by the laser beam⁴². (vi) The electrons are injected into the laser beam by the transverse oscillating laser electric field, so they initially have a large transverse momentum comparable to $a_0 m_e c$ ^{41,43}. (vii) Binary collisions and feedback of the accelerated electrons on the bulk plasma dynamics are negligible. Consequently, the electron dynamics can be modeled by considering a single electron in a combined plane electromagnetic wave representing the laser and a static azimuthal magnetic field representing the plasma magnetic field.

In summary, the key input parameters in our test-electron model formulated in this section are the normalized laser amplitude a_0 , channel current density j_0 , and the initial on-axis electron momentum p_0 .

Energy Gain Estimate

We model the laser pulse as a linearly polarized electromagnetic wave propagating along the x -axis. Its electric and magnetic fields are given by

$$\mathbf{E}_{wave} = -\frac{m_e c}{|e|} \frac{\partial \mathbf{a}_{wave}(\xi)}{\partial t}, \quad (2)$$

$$\mathbf{B}_{wave} = \frac{m_e c^2}{|e|} \nabla \times \mathbf{a}_{wave}(\xi), \quad (3)$$

where $\xi \equiv (ct - x)/\lambda_L$ is the phase variable and $\mathbf{a}_{wave}(\xi) = \mathbf{e}_y a_0 \sin(2\pi\xi)$ is the normalized vector potential, with \mathbf{e}_y being a unit vector. The laser electric field in this setup is polarized along the y -axis. The quasi-static magnetic plasma field sustained by the constant current density j_0 can be written as

$$\mathbf{B}_{channel} = \frac{m_e c^2}{|e|} \nabla \times \mathbf{a}_{channel}, \quad (4)$$

where $\mathbf{a}_{channel} = \mathbf{e}_x \alpha (y^2 + z^2)/\lambda_L^2$. Here we introduced a dimensionless current density

$$\alpha \equiv -\pi \lambda_{L0}^2 j_0 / J_A \quad (5)$$

that is expressed in terms of the Alfvén current $J_A \equiv m_e c^3 / |e|$.

The laser pulse tends to drive flat electron trajectories in the laser polarization plane⁴³, so from now on we set $z \equiv 0$ and study electron motion in the (x, y) -plane only. In the combined fields, $\mathbf{E} = \mathbf{E}_{wave}$ and $\mathbf{B} = \mathbf{B}_{wave} + \mathbf{B}_{channel}$, the electron dynamics with radiation friction (RF) taken into account are governed by the equations

$$\frac{d\mathbf{p}}{dt} = -|e|\mathbf{E} - \frac{c|e|}{\epsilon_e} [\mathbf{p} \times \mathbf{B}] - F_{RF} \frac{\mathbf{p}}{|\mathbf{p}|}, \quad (6)$$

$$\frac{d\mathbf{r}}{dt} = \frac{c^2 \mathbf{p}}{\epsilon_e}, \quad (7)$$

where \mathbf{r} and \mathbf{p} are the electron position and momentum, t is the time and

$$F_{RF} = \frac{\kappa \epsilon_e^2 \mathcal{E}^2}{m_e^2 c^4} \quad (8)$$

quantifies the impact of RF where

$$\kappa = 8\pi^2 e^2 / 3\lambda_L m_e c^2 \approx 7.4 \times 10^{-8}. \tag{9}$$

We consider an electron that starts its motion on the axis of the channel at time t_0 with a large transverse momentum, i.e., $y(t_0) = 0$, $\mathbf{p}(t_0) = (0, p_{y,0} \gg m_e c, 0)$. Then, since we study relativistic motion we retain only terms of leading order in $\varepsilon_e \gg m_e c^2$ in the dynamical RF parameter which can then be expressed as³

$$\mathcal{E}^2 = \left(\frac{e}{m_e c \omega_L} \right)^2 \left(E_{\perp} + \frac{c}{\varepsilon_e} [\mathbf{p} \times \mathbf{B}] \right)^2, \tag{10}$$

where $E_{\perp} = \mathbf{E} - \mathbf{p}(\mathbf{p}\mathbf{E})/\mathbf{p}^2$ is the electric field component perpendicular to the electron momentum. Combining the x and y components of Eq. (6), approximating the momentum as $\mathbf{p} \approx \varepsilon_e/c$, and taking into account that \mathbf{a}_{wave} is a function of ξ alone, we find that

$$\frac{d(R + a_{channel})}{dt} = -F_{RF} \frac{d\xi}{dt}, \tag{11}$$

where we introduced the *dephasing rate* $R = (d\xi/dt)\varepsilon_e \lambda_L / m_e c^3 = (\varepsilon_e - cp_x) / m_e c^2$ quantifying the change of ξ at the electron's instantaneous position. Hence, for vanishing RF ($F_{RF} \rightarrow 0$) the quantity $R + a_{channel} = \text{const.} + \mathcal{O}(F_{RF})$ is an integral of motion, which, in turn, implies that the motion of a relativistic electron with the above introduced initial conditions is confined to transverse displacements smaller than the *magnetic boundary*

$$y \leq y_{MB} := \lambda_L \sqrt{\frac{p_{y,0}}{m_e c \alpha}}. \tag{12}$$

Taking into account RF, however, one finds that for the same initial conditions the magnetic boundary shrinks as a function of time according to

$$y_{MB}(t) = \lambda_L \sqrt{\frac{p_{y,0}}{m_e c \alpha} - \int_{\xi(t_0)}^{\xi(t)} d\xi \frac{F_{RF}}{\alpha}}. \tag{13}$$

The maximum channel potential $a_{channel}$ that can be sampled by the electron also decreases with time and it is limited by $|a_{channel}| \leq |a_{channel}[y_{MB}(t)]|$.

We now turn to studying the electron energy gain. From Eq. (6) we see that it is given by the balance between acceleration and deceleration in the laser field and losses to radiation friction

$$\frac{d\varepsilon_e}{dt} = \sum_{i=x,y,z} \frac{p_i c^2}{\varepsilon_e} \frac{dp_i}{dt} = \frac{m_e c^3 \omega_L}{\varepsilon_e} (p_y \cos(2\pi\xi) a_0 - |\mathbf{p}| F_{RF}). \tag{14}$$

The first term on the right-hand side is the energy exchange between the electron and the transverse laser electric field. It depends on the relative orientation of the transverse electron velocity and the electric field. If the radiation friction is completely negligible, then the rate of the energy gain in an optical laser field ($\lambda_L = 1 \mu\text{m}$) is limited by

$$\frac{d\varepsilon_e}{dt} \lesssim \omega_L a_0 m_e c^2 \sim 10^{-3} a_0 \left[\frac{\text{GeV}}{\text{fs}} \right]. \tag{15}$$

In the absence of the magnetic field, the electron is able to maintain the rate given by Eq. (15) only over a very short time interval due to its rapid dephasing, $R \gg 1$. As the electron slips with respect to the laser wave-fronts, the energy gain changes to an energy loss. The resulting maximum energy remains comparable to the initial electron energy. The azimuthal magnetic field can fundamentally alter the energy exchange with the wave by deflecting the electron radially and thus allowing the transverse electron velocity to remain anti-parallel to the transverse laser electric field. In this regime, the electron continues to gain energy as it slips with respect to the laser pulse. This regime leads to a significant energy gain, but it can only be achieved for a relatively small $p_{y,0}$ ⁴³.

The magnetic field enhances the energy gain due to the deflections only if the electron travel time between the magnetic boundaries at $y = y_{MB}$ and at $y = -y_{MB}$ is comparable to the period of electric field oscillations at the electron location. The travel time is proportional to y_{MB} that in turn scales as $\sqrt{p_{y,0}}$. The consequence of this scaling is that electrons that are injected into the channel with a large transverse momentum are unable to undergo the energy enhancement⁴³. However, the radiation friction causes the magnetic boundary to contract and, as a result, electrons can enter the energy enhancement regime regardless of their initial transverse momentum. We will numerically demonstrate this in the next section of the paper. Our goal here is to estimate how much energy the electrons can gain once the conditions for that become favorable.

To estimate the maximum energy the electron can gain we need an explicit expression for \mathcal{E} , which requires detailed knowledge of the electron motion in the (x, y) -plane. To this end, we note that once the electron is accelerated in the laser's propagation direction its velocity will only make a small angle $\theta \ll 1$ with the x -axis. Taking into account that the electron is ultra-relativistic, we can write $p_y = p \sin(\theta) \approx \varepsilon_e \theta / c$. We use this expression in

Eq. (14) to find that the energy gain is limited by $d\varepsilon_e/dt \lesssim a_0 m_e c^2 \omega \theta - \kappa \varepsilon_e^2 \mathcal{E}^2 / m_e c^2$. We now distinguish the following two cases: (i) If the electron radiates energy mainly due to the laser field's action, then after some algebra one finds from Eq. (10) that

$$\mathcal{E}^2 \approx \mathcal{E}_{laser}^2 := (\theta^4 + \gamma^{-4}) a_0^2 / 4. \quad (16)$$

(ii) If, on the other hand, the radiative losses are dominated by the channel magnetic field one finds from Eq. (10) that

$$\mathcal{E}^2 \approx \mathcal{E}_{channel}^2 := (e |\mathbf{B}_{channel}| / m_e c \omega)^2 \leq a_{MB}^2(t), \quad (17)$$

where

$$a_{MB} = |e \mathbf{B}_{channel}(y_{MB})| / m_e c \omega \quad (18)$$

is the strength of normalized plasma magnetic field at the magnetic boundary $y_{MB}(t)$.

The role of the plasma magnetic field depends on θ , since the contribution of the laser electric and magnetic fields drops as the electron motion becomes more forward directed. This motivates us to introduce a critical angle, defined as

$$\theta_B := \sqrt{2 a_{MB} / a_0}. \quad (19)$$

It follows from Eqs. (16) and (17) that \mathcal{E}^2 and thus the radiation friction are determined by the channel magnetic field for $\theta < \theta_B$. At large angles, $\theta \geq \theta_B$, the radiative losses are determined by the laser field. The energy gain is then given by $d\varepsilon_e/dt|_{laser} \approx 2\pi a_0 m_e c^2 \theta [1 - \kappa \varepsilon_e^2 \theta^3 a_0 / 8\pi m_e^2 c^4]$. Thus, the electron can gain energy only for

$$\theta \leq \theta_{laser} := \left(\frac{8\pi m_e^2 c^4}{\kappa a_0 \varepsilon_e^2} \right)^{\frac{1}{3}}. \quad (20)$$

On the other hand, the radiative losses are determined by the channel magnetic field at $\theta \leq \theta_B$, with the energy gain given by $d\varepsilon_e/dt|_{laser} \approx m_e c^2 (2\pi a_0 \theta - \kappa \gamma^2 a_{MB}^2)$. Consequently, the electron can gain energy in this regime only as long as

$$\theta \geq \theta_{channel} := \frac{\kappa a_{MB}^2 \varepsilon_e^2}{2\pi m_e^2 c^4 a_0}. \quad (21)$$

The qualitative difference between Eqs. (20) and (21) is that at $\theta > \theta_B$ the electron can gain energy only when reducing its propagation angle, whereas at $\theta < \theta_B$ the electron can gain energy only when increasing its propagation angle. This difference indicates that independently of its initial value the electron propagation angle always tends to θ_B . Such an asymptotic behavior, in turn, implies the existence of an upper boundary for the electron energy beyond which further energy gain is prohibited due to radiative losses:

$$\varepsilon_e^{\max} = m_e c^2 \left(\frac{8\pi^2 a_0}{\kappa^2 a_{MB}^3} \right)^{\frac{1}{4}}. \quad (22)$$

This expression for ε_e^{\max} is obtained by setting $\theta_{laser} = \theta_{channel}$ in Eqs. (20) and (21) and solving for the electron energy.

In order to apply Eq. (22) to estimate the maximum electron energy gain in simulations, one should treat a_{MB} as a constant. The value must be set to that at the start of the energy enhancement process, which is likely to be lower than a_{MB} at the beginning of the simulations when the energy gain is not possible. It is shown in Sec. IV that the contraction of the magnetic boundary significantly slows down at the onset of the energy enhancement (see Fig. 2b).

Equation (22) provides an upper estimate for the electron energy in the case when the radiation friction force is included into the equations of motion. In our analysis, the primary channel for the energy losses is the radiation friction. It is important to stress that the electron energy gain can also be limited without the energy losses associated with the radiation friction. A detailed analysis similar to that presented in ref.⁵⁸ is required to determine the corresponding maximum electron energy.

Results

The estimate derived in the previous section states that, when the radiation friction is taken into account, an electron inside the plasma channel can gain energy up to

$$\varepsilon_e^{\max} \approx 5.6 \left(\frac{a_0}{a_{MB}^3} \right)^{\frac{1}{4}} \text{ GeV}, \quad (23)$$

where a_{MB} is the maximum strength of the normalized channel magnetic field experienced by the electron and $\kappa \approx 7.4 \times 10^{-8}$ is a constant calculated for $\lambda_L = 1 \mu\text{m}$. The energy gain is predicted to occur after the magnetic

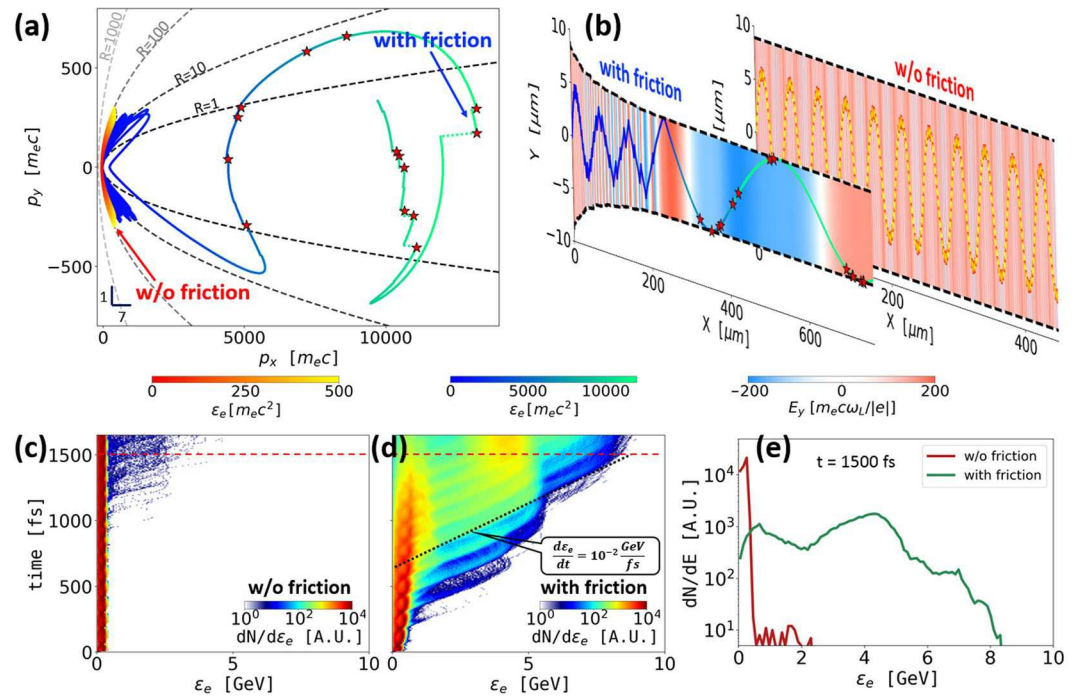


Figure 2. Energy enhancement by the radiation friction. (a) Electron trajectories in the momentum-space with (blue-green) and without (red-yellow) the radiation friction. The stars mark photon emissions with $\epsilon_\gamma > 50$ MeV. (b) Electron trajectories in the (x, y) plane with the energy color-coding the same as in (a). The dashed curves show the magnetic boundary. The background color is the amplitude of the transverse laser electric field at the electron location. (c,d) Time-resolved electron spectra with and without the radiation friction. (e) Electron energy spectra at $t = 1500$ fs [dashed red lines in (c,d)].

boundary contracts sufficiently due to the radiation friction to make the travel time between the magnetic boundaries comparable to period of laser oscillations at the electron location.

In order to investigate this regime, we first consider a single electron with $p_{y,0} = 100 m_e c$ irradiated by a laser pulse with a normalized amplitude $a_0 = 200$ and a wavelength $\lambda_L = 1 \mu\text{m}$. The laser parameters correspond to an intensity of $I_L \approx 5 \times 10^{22} \text{ W/cm}^2$ that is well within the reach of next-generation laser facilities⁷. We set the normalized current density to $\alpha = 1.2$, which corresponds to a 3.2 MA current within a channel whose radius is $4 \mu\text{m}$. The electron starts its motion on axis at the moment when the laser electric field is at its maximum. Figure 2b shows the corresponding electron trajectory calculated without including the radiation friction, with the magnetic boundary marked by a dashed line. The location of the magnetic boundary remains constant in this case. The normalized magnetic field at the boundary is approximately given by $a_{MB} \sim 10^{-2} a_0$. The considered electron experiences very rapid dephasing, which prevents it from gaining significant energy compared to its initial value. The corresponding electron trajectory in the momentum space is shown in Fig. 2a, where the red-yellow color-scheme indicates the electron energy.

The radiation friction qualitatively changes the electron trajectory in Fig. 2b (green-blue color-scheme) and the energy exchange with the field of the laser in Fig. 2a. The radiation friction is simulated by emitting individual photons in the direction opposite to \mathbf{p} according to the synchrotron cross-section, as detailed in Methods. It must be pointed out that the results are similar to those obtained for the continuous radiation friction used in the previous section (see ref.⁵⁹ for a detailed comparison between the classical and QED emission processes). In particular, in the early acceleration phase, which is modeled in the previous section, the emission is apparently quasi-continuous (see Fig. 2), whence the numerical and analytical models give equivalent results. In addition, the discrete photon emission model also captures the correct physics at later times, after the electrons are accelerated to high values of γ and the emission is no longer continuous. As shown in Fig. 2b, the radiation friction causes the magnetic boundary to shrink. Once the boundary shrinks sufficiently to make the travel time across the channel comparable to the period of the electric field oscillations at the electron location, the electron starts gaining energy from the laser. The key feature of the energy gain process is distinctly visible in Fig. 2a, where p_x increases as p_y performs a transverse oscillation. In the absence of the magnetic field deflections, such an oscillation of p_y would prevent the net energy accumulation, as in the earlier part of the trajectory in Fig. 2a.

The maximum electron energy in Fig. 2a is roughly $15000 m_e c^2$ or 7.5 GeV. Our estimate given by Eq. (23) predicts $\epsilon_e^{\text{max}} \sim 10 \text{ GeV}$ for $a_{MB} \sim 10^{-2} a_0$. We thus conclude that Eq. (23) captures the upper limit on the energy gain imposed by the radiation friction relatively well. It is worth pointing out that the contraction of the magnetic boundary significantly slows down once the electrons starts its rapid energy increase accompanied by a reduced phase slip, as seen in Fig. 2b. This result is in agreement with Eq. (13) that states that the shrinking of γ_{MB} is

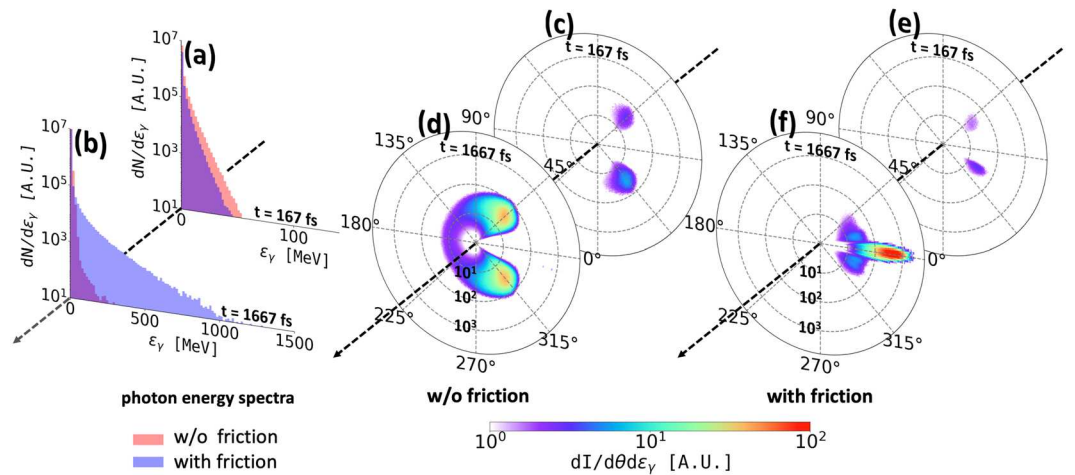


Figure 3. Photon emission with and without the radiation friction. (a,b) Energy spectra of the emitted photons. (c–f) Angular distribution of the emitted photons in the (x, y) -plane. The radial coordinate is the photon energy ε_γ on a log-scale. The polar angle is $\theta_\gamma = \tan^{-1}(p_{\gamma,y}/p_{\gamma,x})$.

determined by the phase slip $\Delta\xi$. It is therefore appropriate to treat a_{MB} in Eq. (23) as a constant when estimating the energy gain.

In order to clearly identify statistically meaningful trends, we consider an ensemble of 10^6 electrons with $p_{y,0}/m_e c \in [40, 160]$. The electrons are uniformly distributed over the specified range of $p_{y,0}$. The time-resolved energy spectra of the electron ensemble shown in Fig. 2c,d further corroborate the beneficial effect of the radiation friction that causes a dramatic energy increase for a large number of the electrons. The energy gain shown by a dotted line in Fig. 2d is roughly $d\varepsilon_e/dt \approx 10^{-2}$ GeV/fs. It is less than what is predicted by Eq. (15) because the electron momentum is directed forward during the acceleration with $|\theta| \ll 1$. The cutoff energy after 1500 fs is $\varepsilon_e \approx 8$ GeV (see Fig. 2e), which is again in reasonable agreement with Eq. (23).

The increase in the electron energies leads to emission of high energy gamma-rays. This aspect is illustrated in Fig. 2 by indicating the emission of photons with energies above 50 MeV ($\varepsilon_\gamma > 50$ MeV). These events occur only after the longitudinal momentum exceeds roughly 5000 $m_e c$, which is the value that the electron is unable to reach in the absence of the radiation friction. The photons are emitted along \mathbf{p} , so they are highly directional because most of the electron momentum is associated with the forward motion. The time-integrated photon energy spectra for the electron ensemble reveal that while at early times the radiation friction does not cause significant differences in the emitted photon pattern (see Fig. 3a), at later times the photon spectrum with the radiation friction stretches to a cut-off energy $\varepsilon_\gamma^{\text{RF}} \sim 1$ GeV, as compared to $\varepsilon_\gamma^{\text{noRF}} \sim 100$ MeV if the radiation friction is neglected (see Fig. 3b). Furthermore, we find the integrated radiation signal at early times to be centered in two lobes at comparable angles $\theta_\gamma \approx \pm 45^\circ$, irrespective of whether the radiation friction is taken into account or not (see Fig. 3c,e), whereas at late times the radiation friction leads to significant collimation of the emitted photons as compared to the case without the radiation friction in which the angular photon distribution preserves the two-lobe structure (see Fig. 3d,f).

Summary and Discussion

We have considered the dynamics of laser-irradiated electrons in a strong quasi-static azimuthal plasma magnetic field. We have demonstrated that the radiation friction can cause a dramatic energy increase. The process consists of two subsequent stages: contraction of the magnetic boundary and enhanced energy gain from the laser field. The contraction of the magnetic boundary reduces the electron travel time across the magnetic filament thus creating the conditions necessary for the energy enhancement. The maximum energy that the electron can gain from the laser pulse before the radiation friction becomes detrimental is given by Eq. (23). In contrast to the pure vacuum acceleration, the energy increase takes place without any increase of the transverse electron oscillations. The benefit of this regime is that it leads to emission of energetic and highly-directional gamma-rays. Our results suggest that this effect could be observed at next-generation laser facilities with a laser beam of a finite width.

Although we approximate the laser pulse by an infinite plane wave, the results are robust and applicable for a pulse of reasonable duration. The electrons considered in the manuscript quickly gain a relativistic longitudinal velocity, so they are able to move with the laser pulse. We find that the electrons slide only between 30 to 50 laser wavelengths with respect to their original location within the laser pulse during the entire simulation that lasts 1667 fs or 500 laser periods. This means that our results should hold for a laser pulse with duration of 170 fs (this is a laser pulse with a wavelength of 1 μm that has 50 wavelengths).

Our result should be viewed as an upper-limit prediction for the electron energy gain. A fully self-consistent particle-in-cell (PIC) simulation is required to determine the role of such aspects as pulse depletion, superluminal phase velocity, and transverse ponderomotive force caused by a finite beam width⁶⁰ for specific target and laser beam parameters. One such simulation showing the energy increase due to the radiation friction is presented in ref.⁶¹. PIC simulations are also required to make predictions for specific laser and target parameters. The example

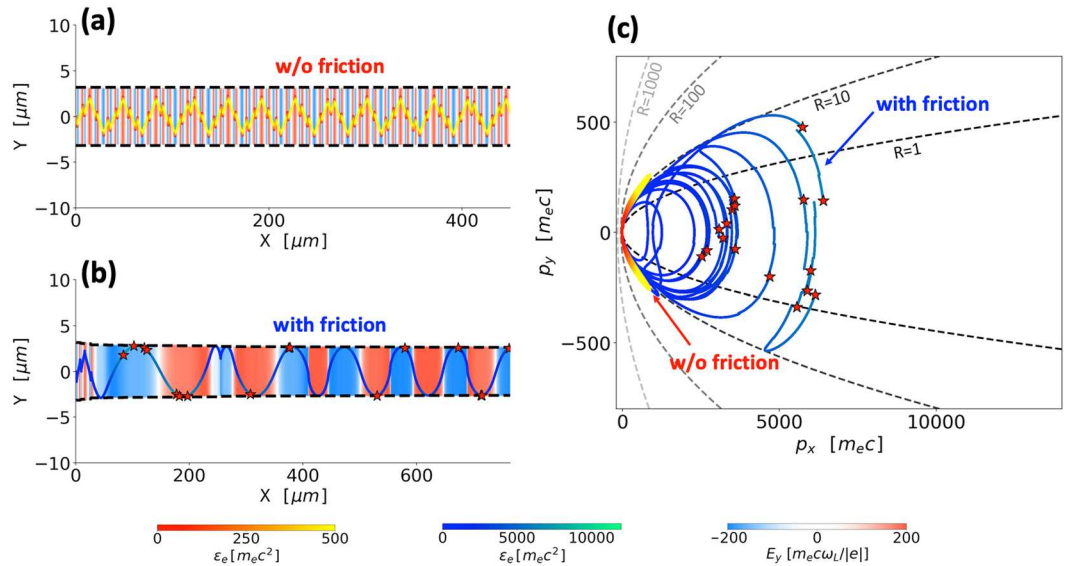


Figure 4. Energy enhancement by the radiation friction for an electron with $p_{y,0} = 40 m_e c$ irradiated by a laser pulse with $a_0 = 200$ inside a magnetic filament sustained by normalized current density $\alpha = 4.0$ defined by Eq. (5).

shown in Fig. 2 is designed to qualitatively illustrate a new effect rather than to constrain laser parameters. It is important to stress that the location of the magnetic boundary and the longitudinal distance needed to achieve the energy enhancement depend on input parameters p_0 and j_0 . In order to illustrate this point, we have performed an additional simulation for an electron with $p_{y,0} = 40 m_e c$ inside a magnetic filament with a normalized current density $\alpha = 4.0$. The results are shown in Fig. 4. In contrast to the example shown in Fig. 2, the magnetic boundary in this case is almost two times closer to the axis, whereas the electron has to travel less than $100 \mu\text{m}$ to experience a significant energy enhancement and start emitting high-energy gamma-rays.

The superluminality is caused by the presence of the plasma, so it imposes a constraint on the electron density. The increase of the phase velocity caused by the plasma that takes into account the relativistically induced transparency can be estimated as $(v_{ph} - c)/c \approx n_e/2a_0 n_c$, where n_e is the electron density. This increase must be less than $(c - v_x)/c$ in order to justify setting $v_{ph} \approx c$. We find that for our electrons we have $(c - v_x)/c \approx 1.2 \times 10^{-3}$, so the corresponding condition reads $(v_{ph} - c)/c < 1.2 \times 10^{-3}$. We have repeated the calculations presented in Sec. IV and found that the changes to the time-resolved electron spectra in Fig. 2d are indeed minimal at $(v_{ph} - c)/c = 10^{-3}$. We thus conclude that the superluminality plays only a secondary role in determining the energy gain if $n_e < n_c$ for the considered laser amplitude of $a_0 = 200$.

Finally, it is important to point out that the discussed regime of the energy enhancement has no hard threshold for a_0 . In contrast to the regimes that require for the Lorentz force to become comparable to the force of the radiation friction^{19,62–64}, our primary requirement is that the contraction of the magnetic boundary should be sufficient during the electron interaction with the irradiating laser pulse to enable the acceleration by the laser electric field. The contraction is described by Eq. (13), so it depends not only on the amplitude of the laser pulse but also on the initial transverse electron momentum. The contraction time reduces with the increase of a_0 , which implies that the discussed regime can be accessed with very short laser pulses of ultra-high intensity.

Methods

We use a fourth-order Runge-Kutta algorithm to push the particle motion under the Lorentz force with the time step $\Delta t = 5 \times 10^{-4} (\lambda_l/c)$ to satisfy the stringent temporal criteria not only on electron acceleration but also on photon generation. We model an infinite plane wave laser field by $E_{\text{wave},y} = a_0 \cos(\xi)$ and $B_{\text{wave},z} = a_0 \cos(\xi)$. The self-generated plasma magnetic field is given by $B_{\text{channel},z} = -2\alpha y$. Since gamma-ray emission to occur over a short distance, the emission probability is calculated under the local constant field approximation^{65–72} by the differential emission rate of an electron with energy ϵ_e and quantum parameter $\chi = E_{rf}/E_{cr}$, where E_{rf} is the electric field in the electron's instantaneous frame and $E_{cr} = m_e^2 c^3 / (e\hbar) \approx 1.3 \times 10^{18} \text{ V/m}^{73}$

$$\frac{d^2 N}{d\chi_\gamma dt} = \sqrt{3} \frac{m_e c^2}{h} \alpha_f \frac{\chi m_e c^2 F(\chi, \chi_\gamma)}{\epsilon_e \chi_\gamma}, \tag{24}$$

where we used the emitted photon's quantum parameter $\chi_\gamma = e\hbar |F_{\mu\nu} k^\nu| / m_e^3 c^3$ and the fine structure constant $\alpha_f = e^2 / 4\pi\epsilon_0 \hbar c \approx 1/137$. The radiated energy is given by⁷³

$$F(\chi, \chi_\gamma) = \frac{4\chi_\gamma^2}{\chi^2} s K_{2/3}(s) + \left(1 - \frac{2\chi_\gamma}{\chi}\right) s \int_s^\infty K_{5/3}(t) dt, \tag{25}$$

where $s = 4\chi_\gamma/[3\chi(\chi - 2\chi_\gamma)]$ and $K_n(s)$ are modified second order Bessel functions. Then each electron is initially assigned a final optical depth $\tau_f = \log[1/(1 - P)]$, with a random number $P \in [0, 1]$ modeling stochastic emission and straggling. The differential rate

$$\frac{d\tau_\gamma}{dt} = \int_0^{\chi/2} \frac{d^2N}{dt d\chi_\gamma} d\chi_\gamma \quad (26)$$

is then advanced over each time step until the assigned optical depth is reached $\tau_\gamma \geq \tau_f$. In the corresponding time step, the electron emits a photon with its specific value χ_γ^f found from the relation

$$\eta = \frac{\int_0^{\chi_\gamma^f} F(\chi, \chi_\gamma)/\chi_\gamma d\chi_\gamma}{\int_0^{\chi/2} F(\chi, \chi_\gamma)/\chi_\gamma d\chi_\gamma}, \quad (27)$$

where $\eta \in [0, 1]$ is a uniformly distributed random number. Then the photon energy, $\hbar\omega_\gamma$, is determined by $\hbar\omega_\gamma = 2m_e c^2 \chi_\gamma^f / \chi$ and the electron's momentum after the emission is given by $\vec{p}^f = [1 - \hbar\omega_\gamma/(cp)]\vec{p}$. Finally, since the gamma-rays are primarily emitted within a cone of opening angle $\Delta\theta \lesssim m_e c^2 / \varepsilon_e$ and we consider $\varepsilon_e \gg m_e c^2$, we assume them to be emitted along the electron's instantaneous direction of motion.

Data availability

All relevant numerical data supporting our findings are available from the corresponding author upon reasonable request.

Received: 6 August 2019; Accepted: 4 November 2019;

Published online: 20 November 2019

References

1. Jackson, J. D. Classical electrodynamics (1999).
2. Dirac, P. A. M. Classical theory of radiating electrons. *Proc. R. Soc. Lond. A* **167**, 148–169 (1938).
3. Landau, L. D. *The classical theory of fields*, vol. 2 (Elsevier, 2013).
4. Strickland, D. & Mourou, G. Compression of amplified chirped optical pulses. *Optics communications* **55**, 447–449 (1985).
5. Mourou, G. A., Tajima, T. & Bulanov, S. V. Optics in the relativistic regime. *Reviews of modern physics* **78**, 309 (2006).
6. Danson, C., Hillier, D., Hopps, N. & Neely, D. Petawatt class lasers worldwide. *High Power Laser Science and Engineering* **3**, e3 (2015).
7. Mourou, G. A., Korn, G., Sandner, W. & Collier, J. L. (editors). *Extreme Light Infrastructure - Whitebook* (Andreas Thoss, 2011).
8. Weber, S. *et al.* P3: An installation for high-energy density plasma physics and ultra-high intensity laser–matter interaction at ebeamlines. *Matter and Radiation at Extremes* **2**, 149 (2018).
9. Di Piazza, A., Müller, C., Hatsagortsyan, K. & Keitel, C. H. Extremely high-intensity laser interactions with fundamental quantum systems. *Reviews of Modern Physics* **84**, 1177 (2012).
10. Bulanov, S. *et al.* On the problems of relativistic laboratory astrophysics and fundamental physics with super powerful lasers. *Plasma Physics Reports* **41**, 1–51 (2015).
11. Wistisen, T. N., Piazza, A., Knudsen, H. V. & Uggerhøj, U. I. Experimental evidence of quantum radiation reaction in aligned crystals. *Nature communications* **9**, 795 (2018).
12. Cole, J. *et al.* Experimental evidence of radiation reaction in the collision of a high-intensity laser pulse with a laser-wakefield accelerated electron beam. *Physical Review X* **8**, 011020 (2018).
13. Poder, K. *et al.* Experimental signatures of the quantum nature of radiation reaction in the field of an ultraintense laser. *Physical Review X* **8**, 031004 (2018).
14. Di Piazza, A., Hatsagortsyan, K. & Keitel, C. Strong signatures of radiation reaction below the radiation-dominated regime. *Physical review letters* **102**, 254802 (2009).
15. Thomas, A., Ridgers, C., Bulanov, S., Griffin, B. & Mangles, S. Strong radiation-damping effects in a gamma-ray source generated by the interaction of a high-intensity laser with a wakefield-accelerated electron beam. *Physical Review X* **2**, 041004 (2012).
16. Harvey, C., Heinzl, T., Ilderton, A. & Marklund, M. Intensity-dependent electron mass shift in a laser field: existence, universality, and detection. *Physical review letters* **109**, 100402 (2012).
17. Neitz, N. & Di Piazza, A. Stochasticity effects in quantum radiation reaction. *Physical review letters* **111**, 054802 (2013).
18. Green, D. & Harvey, C. Transverse spreading of electrons in high-intensity laser fields. *Physical review letters* **112**, 164801 (2014).
19. Gonoskov, A. *et al.* Anomalous radiative trapping in laser fields of extreme intensity. *Phys. Rev. Lett.* **113**, 014801 (2014).
20. Blackburn, T., Ridgers, C., Kirk, J. G. & Bell, A. Quantum radiation reaction in laserelectron-beam collisions. *Physical review letters* **112**, 015001 (2014).
21. Vranic, M., Martins, J. L., Vieira, J., Fonseca, R. A. & Silva, L. O. All-optical radiation reaction at 1 0 21 w/cm². *Physical review letters* **113**, 134801 (2014).
22. Li, J.-X., Hatsagortsyan, K. Z. & Keitel, C. H. Robust signatures of quantum radiation reaction in focused ultrashort laser pulses. *Physical review letters* **113**, 044801 (2014).
23. Dinu, V., Harvey, C., Ilderton, A., Marklund, M. & Torgrimsson, G. Quantum radiation reaction: from interference to incoherence. *Physical review letters* **116**, 044801 (2016).
24. Harvey, C., Gonoskov, A., Ilderton, A. & Marklund, M. Quantum quenching of radiation losses in short laser pulses. *Physical Review Letters* **118**, 105004 (2017).
25. Li, J.-X., Chen, Y.-Y., Hatsagortsyan, K. Z. & Keitel, C. H. Angle-resolved stochastic photon emission in the quantum radiation-dominated regime. *Scientific reports* **7**, 11556 (2017).
26. Geng, X. *et al.* Quantum reflection above the classical radiation-reaction barrier in the quantum electro-dynamics regime. *Communications Physics* **2**, 66 (2019).
27. Pukhov, A., Sheng, Z.-M. & Meyer-ter Vehn, J. Particle acceleration in relativistic laser channels. *Physics of Plasmas* **6**, 2847–2854 (1999).
28. Pukhov, A. Strong field interaction of laser radiation. *Reports on progress in Physics* **66**, 47 (2002).
29. Esarey, E., Schroeder, C. & Leemans, W. Physics of laser-driven plasma-based electron accelerators. *Reviews of modern physics* **81**, 1229 (2009).

30. Arefiev, A. *et al.* Beyond the ponderomotive limit: Direct laser acceleration of relativistic electrons in sub-critical plasmas. *Physics of Plasmas* **23**, 056704 (2016).
31. Zel'Dovich, Y. B. Interaction of free electrons with electromagnetic radiation. *Soviet Physics Uspekhi* **18**, 79 (1975).
32. Fradkin, D. Radiation reaction as a mechanism for increasing energy-momentum of a particle interacting with a laser field. *Physical Review Letters* **42**, 1209 (1979).
33. Meyer-ter Vehn, J. & Sheng, Z. M. On electron acceleration by intense laser pulses in the presence of a stochastic field. *Physics of Plasmas* **6**, 641–644 (1999).
34. Hadad, Y. *et al.* Effects of radiation reaction in relativistic laser acceleration. *Physical Review D* **82**, 096012 (2010).
35. Bashinov, A. V. *et al.* Electron acceleration and emission in a field of a plane and converging dipole wave of relativistic amplitudes with the radiation reaction force taken into account. *Quantum Electronics* **43**, 291–299 (2013).
36. Gelfer, E., Elkina, N. & Fedotov, A. Unexpected impact of radiation friction: enhancing production of longitudinal plasma waves. *Scientific reports* **8**, 6478 (2018).
37. Landau, L. D. & Lifshitz, E. M. *The classical theory of fields* (Pergamon, 1971).
38. Voronin, V. & Kolomenskii, A. The pressure of an intense plane wave on a free charge and on a charge in a magnetic field. *Sov. Phys. JETP* **20**, 1027 (1965).
39. Di Piazza, A. Exact solution of the landau-lifshitz equation in a plane wave. *Letters in Mathematical Physics* **83**, 305–313 (2008).
40. Bulanov, S. V., Esirkepov, T. Z., Kando, M., Koga, J. K. & Bulanov, S. S. Lorentz-abrahamdirac versus landau-lifshitz radiation friction force in the ultrarelativistic electron interaction with electromagnetic wave (exact solutions). *Physical Review E* **84**, 056605 (2011).
41. Stark, D. J., Toncian, T. & Arefiev, A. V. Enhanced multi-mev photon emission by a laserdriven electron beam in a self-generated magnetic field. *Phys. Rev. Lett.* **116**, 185003 (2016).
42. Jansen, O. *et al.* Leveraging extreme laser-driven magnetic fields for gamma-ray generation and pair production. *Plasma Physics and Controlled Fusion* **60**, 054006 (2018).
43. Gong, Z. *et al.* Forward sliding-swing acceleration: electron acceleration by high-intensity lasers in strong plasma magnetic fields. *arXiv preprint arXiv:1811.00425* (2018).
44. Akhiezer, A. & Polovin, R. Theory of wave motion of an electron plasma. *Sov. Phys. JETP* **3**, 696–705 (1956).
45. Kaw, P. & Dawson, J. Relativistic nonlinear propagation of laser beams in cold overdense plasmas. *The Physics of Fluids* **13**, 472–481, <https://doi.org/10.1063/1.1692942> (1970).
46. Gibbon, P. *Short pulse laser interactions with matter* (World Scientific Publishing Company, 2004).
47. Palaniyappan, S. *et al.* Dynamics of relativistic transparency and optical shuttering in expanding overdense plasmas. *Nature Physics* **8**, 763 (2012).
48. Fernández, J. C. *et al.* Laser-plasmas in the relativistic-transparency regime: Science and applications. *Physics of plasmas* **24**, 056702 (2017).
49. Pukhov, A. & Meyer-ter Vehn, J. Relativistic magnetic self-channeling of light in near-critical plasma: three-dimensional particle-in-cell simulation. *Physical review letters* **76**, 3975 (1996).
50. Lasinski, B. F., Langdon, A. B., Hatchett, S. P., Key, M. H. & Tabak, M. Particle-in-cell simulations of ultra intense laser pulses propagating through overdense plasma for fast-ignitor and radiography applications. *Physics of Plasmas* **6**, 2041–2047 (1999).
51. Nakamura, T., Bulanov, S. V., Esirkepov, T. Z. & Kando, M. High-energy ions from nearcritical density plasmas via magnetic vortex acceleration. *Physical review letters* **105**, 135002 (2010).
52. Bulanov, S. S. *et al.* Generation of gev protons from 1 pw laser interaction with near critical density targets. *Physics of plasmas* **17**, 043105 (2010).
53. Liu, B. *et al.* Generating overcritical dense relativistic electron beams via self-matching resonance acceleration. *Physical review letters* **110**, 045002 (2013).
54. Huang, T. *et al.* Relativistic laser hosing instability suppression and electron acceleration in a preformed plasma channel. *Physical Review E* **95**, 043207 (2017).
55. Snyder, J. *et al.* Relativistic laser driven electron accelerator using micro-channel plasma targets. *Physics of Plasmas* **26**, 033110 (2019).
56. Williams, J. Private communications at General Atomics (2019).
57. Willingale, L. *et al.* The unexpected role of evolving longitudinal electric fields in generating energetic electrons in relativistically transparent plasmas. *New Journal of Physics* **20**, 093024 (2018).
58. Khudik, V., Arefiev, A., Zhang, X. & Shvets, G. Universal scalings for laser acceleration of electrons in ion channels. *Physics of Plasmas* **23**, 103108, <https://doi.org/10.1063/1.4964901> (2016).
59. Di Piazza, A., Hatsagortsyan, K. & Keitel, C. H. Quantum radiation reaction effects in multiphoton compton scattering. *Physical review letters* **105**, 220403 (2010).
60. Ji, L., Pukhov, A., Kostyukov, I. Y., Shen, B. & Akli, K. Radiation-reaction trapping of electrons in extreme laser fields. *Physical review letters* **112**, 145003 (2014).
61. Vranic, M., Fonseca, R. A. & Silva, L. O. Extremely intense laser-based electron acceleration in a plasma channel. *Plasma Physics and Controlled Fusion* **60**, 034002 (2018).
62. Chen, M., Pukhov, A., Yu, T.-P. & Sheng, Z.-M. Radiation reaction effects on ion acceleration in laser foil interaction. *Plasma Physics and Controlled Fusion* **53**, 014004 (2010).
63. Tamburini, M., Pegoraro, F., Di Piazza, A., Keitel, C. H. & Macchi, A. Radiation reaction effects on radiation pressure acceleration. *New Journal of Physics* **12**, 123005 (2010).
64. Bulanov, S. *et al.* Charged particle dynamics in multiple colliding electromagnetic waves. survey of random walk, lévy flights, limit circles, attractors and structurally determinate patterns. *Journal of Plasma Physics* **83** (2017).
65. Bell, A. & Kirk, J. G. Possibility of prolific pair production with high-power lasers. *Physical review letters* **101**, 200403 (2008).
66. Sokolov, I. V., Nees, J. A., Yanovsky, V. P., Naumova, N. M. & Mourou, G. A. Emission and its back-reaction accompanying electron motion in relativistically strong and qed-strong pulsed laser fields. *Physical Review E* **81**, 036412 (2010).
67. Duclous, R., Kirk, J. G. & Bell, A. R. Monte carlo calculations of pair production in highintensity laser–plasma interactions. *Plasma Physics and Controlled Fusion* **53**, 015009 (2010).
68. Elkina, N. *et al.* Qed cascades induced by circularly polarized laser fields. *Physical Review Special Topics-Accelerators and Beams* **14**, 054401 (2011).
69. Ridgers, C. *et al.* Modelling gamma-ray photon emission and pair production in high-intensity laser–matter interactions. *Journal of Computational Physics* **260**, 273–285 (2014).
70. Gonoskov, A. *et al.* Extended particle-in-cell schemes for physics in ultrastrong laser fields: Review and developments. *Physical Review E* **92**, 023305 (2015).
71. Green, D. & Harvey, C. Simla: Simulating particle dynamics in intense laser and other electromagnetic fields via classical and quantum electrodynamics. *Computer Physics Communications* **192**, 313–321 (2015).
72. Harvey, C., Ilderton, A. & King, B. Testing numerical implementations of strong-field electrodynamics. *Physical Review A* **91**, 013822 (2015).
73. Ritus, V. J. *Rus. Las. Res* **6**, 497 (1985).

Acknowledgements

This research was supported by NSF (Grants No. 1632777 and 1821944), AFOSR (Grant No. FA9550-17-1-0382), the National Basic Research Program of China (Grant No. 2013CBA01502), and NSFC (Grant No. 11535001). Z.G. was partly supported by the scholarship from China Scholarship Council (CSC) under the Grant CSC No. 201706010038.

Author contributions

All authors together came up with the original idea, designed the setup and discussed the effect. Z.G. performed the numerical simulations, F.M. and A.V.A. developed the analytical model, Z.G., F.M. and A.V.A. wrote the manuscript. A.V.A. guided and supervised the project.

Competing interests

The authors declare no competing interests.

Additional information

Correspondence and requests for materials should be addressed to A.V.A.

Reprints and permissions information is available at www.nature.com/reprints.

Publisher's note Springer Nature remains neutral with regard to jurisdictional claims in published maps and institutional affiliations.



Open Access This article is licensed under a Creative Commons Attribution 4.0 International License, which permits use, sharing, adaptation, distribution and reproduction in any medium or format, as long as you give appropriate credit to the original author(s) and the source, provide a link to the Creative Commons license, and indicate if changes were made. The images or other third party material in this article are included in the article's Creative Commons license, unless indicated otherwise in a credit line to the material. If material is not included in the article's Creative Commons license and your intended use is not permitted by statutory regulation or exceeds the permitted use, you will need to obtain permission directly from the copyright holder. To view a copy of this license, visit <http://creativecommons.org/licenses/by/4.0/>.

© The Author(s) 2019